Rapid directivity detection by azimuthal amplitude spectra inversion

Simone Cesca, Sebastian Heimann, Torsten Dahm

Simone Cesca, Sebastian Heimann, Torsten Dahm. Rapid directivity detection by azimuthal amplitude spectra inversion. Journal of Seismology, Springer Verlag, 2010, 15 (1), pp.147-164. 10.1007/s10950-010-9217-4 . hal-00642936

J Seismol
DOI 10.1007/s10950-010-9217-4

ORIGINAL ARTICLE

Rapid directivity detection by azimuthal amplitude spectra inversion

Simone Cesca · Sebastian Heimann · Torsten Dahm

Received: 24 February 2010 / Accepted: 4 November 2010

Abstract An early detection of the presence of rupture directivity plays a major role in the correct estimation of ground motions and risks associated to the earthquake occurrence. We present here a simple method for a fast detection of rupture directivity, which may be additionally used to discriminate fault and auxiliary planes and have first estimations of important kinematic source parameters, such as rupture length and rupture time. Our method is based on the inversion of amplitude spectra from P-wave seismograms to derive the apparent duration at each station and on the successive modelling of its azimuthal behaviour. Synthetic waveforms are built assuming a spatial point source approximation, and the finite apparent duration of the spatial point source is interpreted in terms of rupture directivity. Since synthetic seismograms for a point source are calculated very quickly, the presence of directivity may be detected within few seconds, once a focal mechanism has been derived. The method is here first tested using synthetic datasets, both for linear and planar sources, and then successfully applied to recent Mw 6.2–6.8 shallow earthquakes in Peloponnese, Greece. The method is suitable for automated application and may be used to improve kinematic waveform modelling approaches.

Keywords Directivity · Earthquake source · Kinematic model · Amplitude spectra

1 Introduction

Tectonically driven shallow earthquake sources are generally explained by means of shear cracks occurring along a limited, almost planar region, we refer as the focal region. A point source representation is a common first approximation, which is valid when treating far-field low frequency seismic waveform, using wavelengths larger than the rupture size. Higher frequencies seismograms and spectra contain information which can be related to the finiteness of the rupture process and thus can be used to determine parameters describing the finite source. Size and shape of the rupture area, rupture velocity and preferential rupture directions, an effect known as rupture directivity, are some of the parameters which can be retrieved by the analysis of high-frequency waveforms. In particular, we are interested here in discussing the problem of early detection of rupture directivity, distinguishing between a prominent or partial unilateral rupture (a case which will be further referred as asymmetric bilateral rupture), and a

S. Cesca (✉) · S. Heimann · T. Dahm
Institut für Geophysik, Universität Hamburg,
Bundesstrasse 55, 20146 Hamburg, Germany
e-mail: simone.cesca@zmaw.de

bilateral one, with rupture nucleating at the centre of the rupture area and propagating toward its edges. The azimuthal dependency of amplitudes and durations of different seismic phases is a first indicator of directivity effects and is consequence of the characteristics of the finite rupture process along the fault plane, specifically the main direction and speed of the rupture front propagation. Directivity has been often observed and has been modelled for several earthquakes in the past, with several studies treating specific earthquakes or limited datasets (e. g., McGuire et al. 2002; Warren and Shearer 2006; Caldeira et al. 2009). A quick detection of directivity effects is important towards a correct estimation of ground motions, stress field perturbations and tsunamogenic risks and consequently to mitigate earthquake effects. These considerations provide important reasons to further investigate and develop specific tools for stable, rapid and automated directivity detection, which can be used within early warning systems.

Several methods have been applied in the past to detect and classify earthquake source directivity. A common approach is the identification of predominant unilateral ruptures from the time duration and spectral analysis of body wave pulses (e.g. Boore and Joyner 1978; Beck et al. 1995; Warren and Shearer 2006; Caldeira et al. 2009). Pulse lengths at different stations are interpreted in terms of the apparent duration of the source time function (STF), and their variation in dependence on azimuth and incidence angle is interpreted to detect directivity: similarly to a Doppler effect in classical physics, shorter STFs would indicate a rupture propagating towards the considered station, while longer pulses indicate a rupture propagation in the opposite direction. Directivity effects may also be revealed based on the analysis of surface waves at different azimuths (Ben-Menahem 1961; Pro et al. 2007). Whereas time domain methods remain more common, a significant contribution within this type of inversion methods was provided by the spectral approach discussed in Warren and Shearer (2006). This method is based on the spectral estimation of the pulse broadening and accounts for the azimuthal and incidence angle dependencies; it is well suited for the analysis of intermediate and deep focus earthquakes and was successfully applied to several events. The main limits of this class of methods are related to the fact that wave propagation and the superposition of different seismic phases are not accounted, since wave propagation effects between source and receiver (Green's functions) are limited to the estimation of the incidence angle of given seismic phases. Another possible limitation is the requirement of several stations with good azimuthal coverage in order to ensure reliable results. A second range of applications, which on the contrary accounts precisely for the effects of the earth's model on the observed waveforms, is based on empirical Green's functions technique (Hartzell 1978; Li and Toksöz 1993; Velasco et al. 1994; Cassidy 1995; Müller 1985; Velasco et al. 2004; Vallée 2007). In this case, an aftershock with common hypocenter and focal mechanism of the studied event can be used to remove path effects, and isolate finite source apparent durations at different stations. Evidently, the application of these techniques is strongly limited by the availability of a proper aftershock. Brüstle and Müller (1987), and Imanishi and Takeo (2002) have investigated the adoption of master-event techniques to detect directivity: the identification of stopping phases (Madariaga 1977, 1983; Bernard and Madariaga 1984; Spudich and Frazer 1984) at different stations was used there to determine the main direction of rupture propagation, besides other source properties. Stopping phases identification (Imanishi and Takeo 1998, 2002) typically requires a careful waveform analysis, which may be hardly implemented within automated routines. A third group of techniques are based on complete kinematic waveform inversion, with the aim of retrieving a most detailed image of the finite rupture process, not limited to the identification of directivity. The range of methods and applications is very wide, including higher order moment tensor analysis (Dahm and Krüger 1999; McGuire et al. 2001, 2002), detailed slip map approaches (e.g. Olson and Apsel 1982; Hartzell and Helmberger 1982; Hartzell and Heaton 1983; Beroza and Spudich 1988), and inversion methods adopting constrained and simplified kinematic models (Dreger and Kaverina 2000; Vallée and Bouchon 2004; Gallovic et al. 2009; Cesca et al.

2010). All these methods have a significant potential for a stable determination of directivity but their adoption towards its very fast detection is limited, often requiring time consuming computation of synthetic seismograms for several extended source models. Methods developed by Dreger and Kaverina (2000) and following Cesca et al. (2010) have shown a good performance and have been tested for near real-time applications, but they are still based on extended source representations and thus require heavier computations with respect to our method. Finally, recent results by Zahradnik et al. (2008) showed the possibility of discriminating the true fault plane on the base of spatial offsets between epicentre and centroid locations. However, the method has been currently applied only to a limited number of earthquakes, with variable results, and the determination of directivity may be beyond its possibilities, for example for symmetric bilateral ruptures.

We present here a simple alternative method to quickly detect directivity for shallow earthquakes and discuss it with the aid of a set of applications, including both synthetic datasets and observations from recent earthquakes in Greece. Our method is based on a point source representation, which drastically reduces computational requirements and makes it feasible for early detection. Directivity is detected on the basis of a frequency domain inversion of the apparent duration at each station and the further interpretation of its azimuthal variation. Main strength points of the proposed method include the adoption of a common dataset and modelling tools for focal mechanism and directivity determination, the inclusion of Green's functions accounting for wave propagation through the chosen earth models without needing specific aftershocks, and the simplicity and quickness of the inversion process.

2 Directivity and amplitude spectra inversion

We make here use of the recently developed Kiwi tools (Heimann 2010; Cesca et al. 2010; http://kinherd.org), which provide a flexible instrument to generate synthetic seismograms for point and extended sources and to invert different earthquake source parameters, allowing the selection of different waveform tapers, frequency filters, inversion domains and misfit functions. Cesca et al. (2010) showed successful applications to shallow earthquake at regional distances, and was able to derive both point source (best double couple, DC, model, scalar moment and centroid depth) and extended source (fault plane discrimination, rupture size, rupture time, rupture nucleation) parameters.

The first inversion step follows the approach described in Cesca et al. (2010), to obtain the focal mechanism, scalar moment and centroid depth:

1. Focal mechanism. We invert amplitude spectra of full waveforms, according to Cesca et al. (2010), to derive a point source focal mechanism (DC, depth and scalar moment); the source epicentral location is assumed to be originally known.
2. Polarities. The focal mechanism presents a polarity ambiguity, which can be solved by comparing observed displacements and synthetic seismograms for the two possible polarity configurations; however, the detection of the true polarity is here not strictly required, as the whole inversion process is carried out in the frequency domain, and only amplitude spectra are involved in the fitting procedure.

The source representation through the Kiwi tools allows the adoption of different rise times. For a spatially extended source model, where the rupture region is discretised into a number of spatial point sources, the rise time represent the time during which each point source radiates seismic energy. The duration of the whole rupture process is related to rise and rupture times. If we adopt a point source representation, the rise time will represent the duration of the source time function. This parameter was used in Cesca et al. (2010) to have a first, rough, estimate of rupture times and to choose a proper rise time during kinematic source modelling. We proceed here differently: instead of determining true duration of the rupture process, we investigate apparent durations as seen by individual stations.

In detail, during the second inversion step, we proceed as follows (Fig. 1 illustrates an example of the main steps, relative to selected seismic

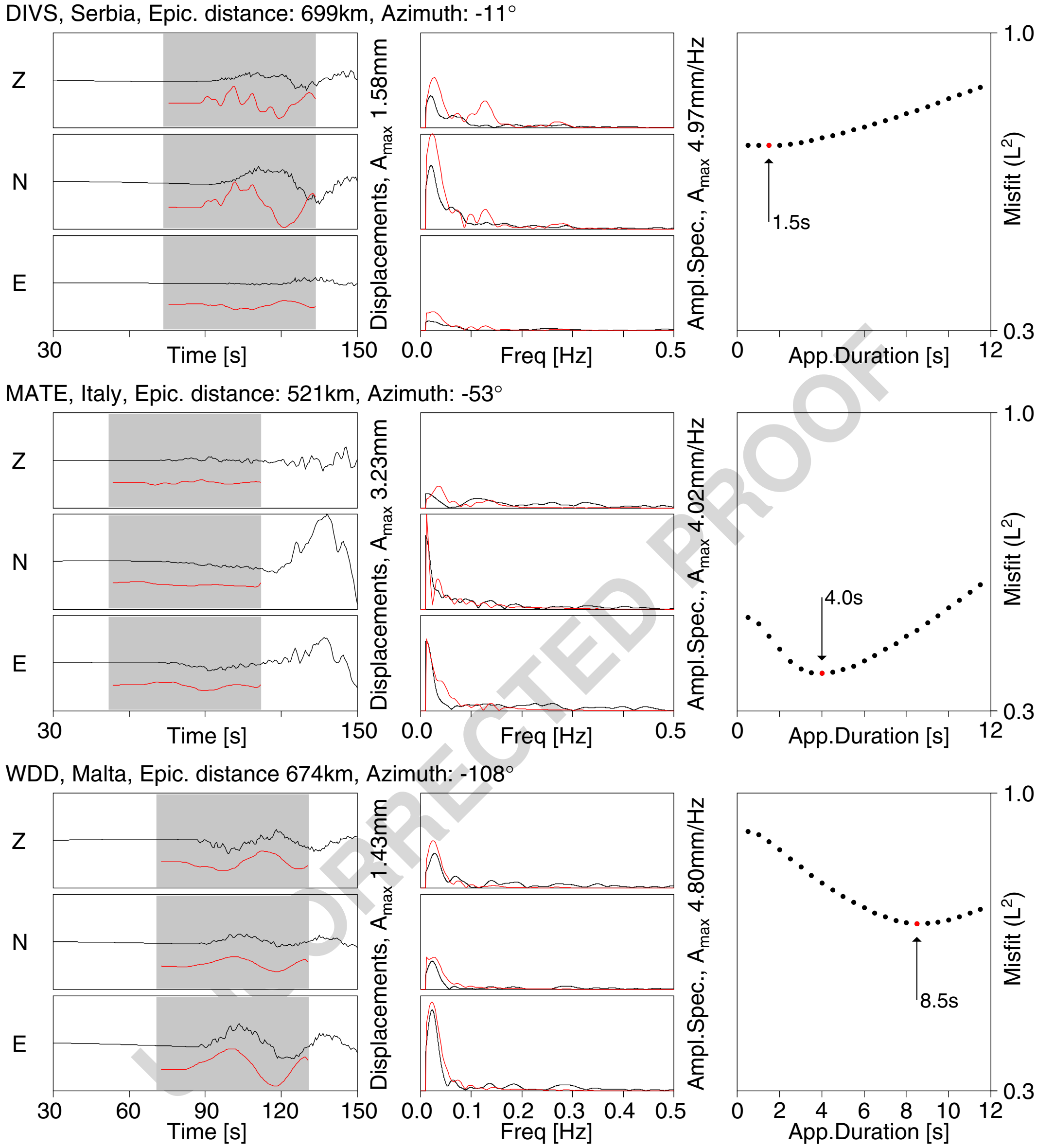

Fig. 1 Example of the procedure followed to derive the apparent source duration at different stations. Selected waveforms, spectra and amplitude spectra inversion results refer to an application to the Andravida earthquake, Greece, which is further extensively discussed in this study. *Left*: filtered displacements (*black lines*) and synthetic seismograms (*red lines*) for the chosen point source model are tapered to select P waves time windows (*grey intervals*). *Centre*: amplitude spectra comparison (*red lines* correspond to the best fitting synthetic spectra, after comparing several source durations). *Right*: comparison of amplitude spectra misfit values for different source durations (best solutions for each station are identified by *red circles*)

waveforms from the Andravida earthquake, which is later discussed in the text):

1. Waveform selection. We use all available spatial components, preferably using North, East and vertical orientations, rather than rotated traces, in order to have P wave energy on all traces (which is theoretically null on transversal components); the presence of more traces for each station has a smoothing effect; after

testing with different datasets, we found that more components provide more stability. We perform a deconvolution of the instrumental response from the data, and conversion to displacements.

2. Tapering. We limit the inversion process to P-wave time windows, which are automatically selected on the base of the source-receiver geometry and theoretical arrival time for the earth model used during the inversion (an arrival time database is calculated in advance, to reduce computational effort at the time of the inversion); for the case studies here described we use 60 s length time windows, starting 15 s before theoretical first P arrival, and apply a bandpass filter in the range 0.01–0.5 Hz (these parameters may be modified depending on the earthquake size, the source depth, the average duration, and the range of epicentral distances where waveforms are inverted). Tapers should be chosen in order to resolve directivity effects. A minimum length should account at least for two times the average rupture duration and for different periods at the frequency range used for the inversion. For stations located at small epicentral distances, with minor delay between S and P phases, tapers may be modified to avoid S waves.
3. Scalar moment inversion. Since the estimation of the scalar moment may slightly vary depending on the inversion approach (e.g., full waveform or body waves, time domain or amplitude spectra inversion, etc.), we mention here the possibility to perform a specific inversion using an approach consistent with the following directivity inversion. Traces from all seismic stations would be used to invert the scalar moment (e.g. by amplitude spectra inversion, using a Levenberg–Marquardt approach and an L^2 norm misfit function). In the following applications this step is not performed, as we count with stable estimations of the scalar moments, provided by the fit of low frequency amplitude spectra from the whole waveforms.
4. Apparent duration inversion. For each of the stations, we perform an amplitude spectra inversion to derive the apparent source duration at that station; the frequency domain inversion approach is less sensitive to unmodelled structural heterogeneities; we perform here a grid search for possible durations (for the following case studies, tested durations varies up to 30 s, with an increment of 0.5 s); in general we observe smooth single-minimum curves of misfit versus apparent durations, and tests with different inversion approaches (e.g. gradient methods) have shown very consistent results with respect to the grid walk procedure.

The apparent source time function durations can be then quickly interpreted in term of simplified laws for finite rupture models. With the aid of synthetic tests and application to selected earthquake datasets, we will show that, often, it is not necessary to have a complex rupture model to fit the azimuthal distribution of apparent durations. For simple extended source model, such as a one-dimensional linear source or a Haskell bidimensional rupture model (Haskell 1964), the effects of directivity can be treated analytically. A unilateral rupture along a horizontal linear source will produce theoretical P-wave pulses of shorter duration for stations located toward the rupture propagation, and larger duration for stations in the opposite direction. Bilateral ruptures result in a minor azimuthal variation of the apparent source time function. A range of asymmetrically bilateral rupture models exists in between. Effects of oblique and vertical rupture propagations may also be modelled but are more difficult to reveal (Beck et al. 1995) and have been more rarely observed (e.g. Eshghi and Zare 2003; Nadim et al. 2004).

We originally focus on the two-dimensional problem, with source and observer laying on the same plane. Let us assume a horizontal linear source model of length L, with the rupture starting at one edge (A) and propagating unilaterally till the other edge (B). The rupture time t_R is the time required for the rupture front to propagate along the entire rupture length, from A to B, at a rupture velocity v_R, which is assumed to be constant. The rise time t_r, defined as the duration of seismic source emission from a point along the source, is here assumed to be constant, according to healing front theory (Nielsen and Madariaga 2003) and will be further considered negligible with respect to the rupture time. Finally, v_P is the average P wave velocity at the focal region. Typically, rupture propagates with a velocity slightly below the shear wave velocity at the focal region, which also shows a common scale with compressional wave velocity in seismogenic regions. Then, according to Ben-Menahem and Singh (1981), and including the rise time, for a receiver located at azimuth φ (defined with respect to the direction of rupture propagation) the apparent source duration $\Delta t(\varphi)$ will be given by:

$$\Delta t\left(\varphi\right) = t_r + \frac{L}{v_R} - \frac{L}{v_P}\cos\left(\varphi\right). \tag{1a}$$

In view of a more general formulation, also accounting for asymmetric and pure bilateral rupture, the rupture length L is divided into two segments L_1 and L_2, with the following expression for the apparent source duration $\Delta t(\varphi)$:

$$\begin{aligned}\Delta t\left(\varphi\right) \;=\; \mathrm{Max}\big[&t_r + L_1/v_R - \left(L_1/v_P\right)\cos\left(\varphi\right), \\ &t_r + L_2/v_R + \left(L_2/v_P\right)\cos\left(\varphi\right)\big]\end{aligned} \tag{1b}$$

We can then introduce the following non-dimensional variables: $\tau(\varphi)$ is the ratio between the apparent source duration $\Delta t(\varphi)$ and the rupture time t_R, $t_{r/R}$ is the ratio between rise and rupture time, $v_{R/P}$ is the ratio between rupture velocity and P wave velocity at the source; L_1 and L_2 ($L_1 \geq L_2$) are expressed as (1-χ)L and χL, respectively, χ being the ratio between the shortest segment and the entire rupture length (χ may range from 0, for a pure unilateral rupture, to 0.5, for a pure bilateral one). The azimuthal dependency of $\tau(\varphi)$, making use of the non-dimensional notation is the following ($t_{r/R}$ can be in general neglected):

$$\begin{aligned}\tau\left(\varphi\right) = \mathrm{Max}\big[&t_{r/R} + 1 - v_{R/P}\cos\left(\varphi\right), \\ &t_{r/R} + L_2/L_1 + L_2/L_1\cos(\varphi)\big].\end{aligned} \tag{2}$$

The radiation pattern for three significant cases (pure unilateral, pure bilateral and asymmetric bilateral) is shown in Fig. 2, where we have chosen $v_{R/P} = 0.5$ ($v_{R/P}$ equal to 0.25 and 1.0 for the slow and fast cases respectively), χ is equal to 0, 1/3 and 1/2 for the three considered cases. We choose different rupture lengths L, in order to have a constant length of the largest rupture segment. Symmetries of apparent duration radiation patterns can be observed, with a one lobe shape for a pure unilateral rupture and a two lobe shape for a pure bilateral one. The theoretical curve of the apparent rupture duration (Fig. 2, right) for the unilateral case range from $t_r + t_R - t_P$ (azimuth of rupture direction) to $t_r + t_R + t_P$ (opposite direction); its average value is equal to $t_r + t_R$ (for a unilateral rupture model t_R and t_P are the rupture time and P wave travel time along the entire rupture length). For the pure bilateral rupture, the apparent duration varies between $t_r + t_R$ (perpendicular to rupture direction) to $t_r + t_R + t_P$ (parallel to rupture direction), with t_R and t_P referring here to half of the rupture length. The larger variation of the apparent duration for the unilateral case, with respect to the bilateral, explains the major difficulties in observing directivity for the second case. Less known is the behaviour of asymmetric bilateral ruptures, although this model is the most general. In this case the radiation pattern (Fig. 2, bottom) present a deformed one-lobe shape, with the minimum observed apparent rupture duration at about 45° from the rupture direction of the largest rupture length. The azimuth α, where a cusp-like minimum in the apparent duration may be observed, can be obtained by equalizing the two right terms in Eq. 2:

$$\alpha = a\cos\left[\frac{(1-2\chi)}{v_{R/P}}\right]. \tag{3}$$

Since v_R pertains to [0, v_P], it follows that for a pure unilateral rupture ($\chi = 0$) we have a single minimum in direction of rupture propagation, while cusp-like minima are not observed. For a pure bilateral rupture ($\chi = 0.5$), $\alpha = \pm\pi/2$ always. For the intermediate case of asymmetric bilateral ruptures ($0 < \chi < 0.5$), two cusp-like minima are observed if the following condition is met:

$$\chi > \frac{\left(1/v_{R/P}\right)}{2}. \tag{4}$$

This means that the observation of two minima in the apparent duration curve indicate a dominant bilateral rupture processes.

Figure 2 additionally shows how larger variations in the apparent duration estimations are found, when increasing the rupture velocity (in the figure, effects for an extreme case of $v_R =$

Fig. 2 Theoretical models for pure unilateral (*top*), pure bilateral (*centre*) and asymmetric bilateral (*bottom*) line sources. The ruptures start at a nucleation point (*white circles*, *left plots*) and propagate along segments L_1 and L_2 (*black arrows*), producing different apparent duration radiation patterns (*grey regions*, *central plots*) which have an azimuthal dependence. *Right plots* present the curves of the apparent duration versus azimuth: *thick black lines* represent an average behaviour ($v_R = 0.5v_P$), while *dashed lines* represent fast ($v_R = v_P$) and slow ($v_R = 0.25v_P$) rupture cases. In the case of a partial unilateral rupture, the curve of apparent duration for the average case (*thick black line*) is given by the maximum of the curves associated to unilateral ruptures along the two segments (*thick grey lines*)

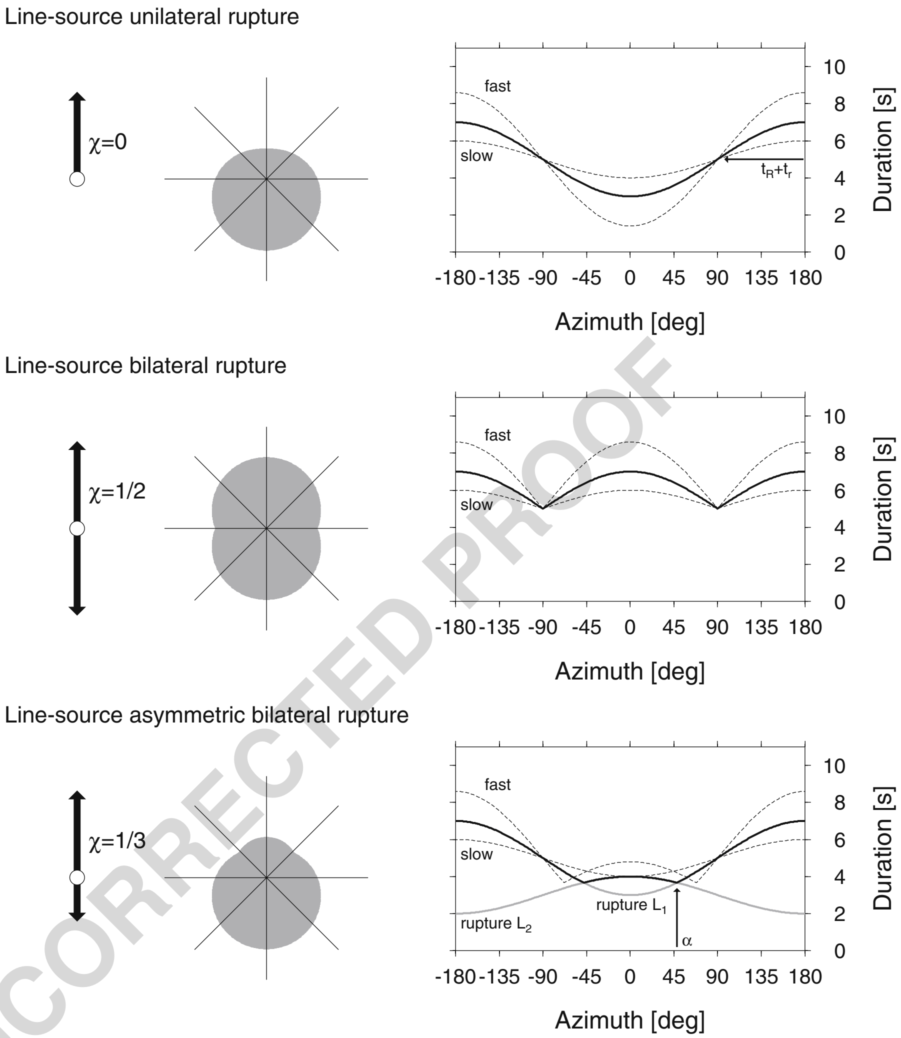

v_P are considered). On the other hand, a slower rupture tends to behave similarly to a spatial point source model (with a finite time duration); Fig. 2 shows the case of $v_R = 0.25v_P$, a proportion which is not unrealistic and can be proper for shallow earthquake in sediment layers (e.g. Selby et al. 2005; Dahm et al. 2007).

For a 3D earth model, directivity effects do not depend only on station azimuth but also on take-off angles. Equations 1a, 1b and 2 will then depend on the angle between the rupture direction and the ray direction at the source, instead than on station azimuth. These considerations opened space for specific detailed inversion approaches, such as the successful study by Warren and Shearer (2006), which accounted for take off angles and required a dense station distribution both in terms of azimuthal coverage and range of epicentral distances. We discuss here the problem for the case of unilateral rupture. A first observation is that even for the same source-receiver configuration, different rays travelling along different paths, with different take-off angles, will present different directivity effects. For any considered bodywave with take-off angle θ, we predict theoretically a minor variability of the apparent duration with respect to the one modelled for a planar case. For example, the maximal apparent duration, at the azimuth opposite to the direction of the rupture propagation, will be equal to $t_r + t_R + t_P \cos(\theta)$, which differs from Eq. 1a. Additionally, we have the superposition of different P wave arrivals, with different take-off angles. In any case, the interpretation of the maximal apparent duration following Eq. 1a and neglecting take-off angles and rise time effects will lead to an overestimation of the terms t_R and t_P and consequently an overestimation of the rupture length. The value derived in such approximation can be safely considered as an upper bound to the real rupture length.

Our approach here is to model only the azimuthal variation of directivity effects. The approximation is limited by different conditions. First, we will focus on shallow earthquakes and use only regional distances seismograms (epicentral distances in the range 200–1,000 km), basing our inversion on the fit of time windows centred at the first P wave arrivals. Additionally, we will consider only the case of horizontal to sub-horizontal ruptures (rupture propagating along direction dipping at most 20°). In these circumstances, we will show that the main rupture propagation can be detected even with the approximated approach here described. The interpretation of additional rupture parameters is strongly limited by neglecting take-off angles and rise time effects, and the derived rupture length should be considered as an upper bound to its real value.

On the base of the previous discussion, we can now explain the last step of the inversion approach, where the distribution of apparent source time durations is interpreted in terms of simplified rupture models:

1. Point source model. If we assume a spatial point source model, with a given source time function of duration t_r, the curve of apparent duration will be a straight line, with no azimuthal dependence. This is the particular case, which can also be described by the previous equations, with L = 0, which leads to $t_R = t_P = 0$. The model has a unique unknown, t_r (by definition, rise time), which represents the apparent rupture time everywhere.
2. Pure/predominant unilateral rupture. In this case, the azimuthal distribution of apparent durations is expected to follow a sinusoidal behaviour. The fit is expected to be larger in case of a pure unilateral rupture, but the model can still well reproduce data also for asymmetric bilateral ruptures. In both cases, the minimum of the curve will indicate the main rupture direction (φ_0). The model is represented by the curve of the apparent duration $\Delta t(\varphi)$:

$$\Delta t\,(\varphi) = -A\cos\,(\varphi - \varphi_0) + B \tag{5}$$

with A and B positive, describing in first approximation the travel time of P waves along the rupture length (t_P) and the sum of rise and rupture times ($t_r + t_R$).

3. Pure bilateral rupture. In case of a pure bilateral rupture, we will use the following curve, instead:

$$\Delta t\,(\varphi) = A\,|\cos\,(\varphi - \varphi_0)| + B. \tag{6}$$

4. Comparison of directivity models. Since Eqs. 5 and 6 are dependent on three unknown parameters, while the standard average rupture time has only one (the average earthquake duration or duration of the common source time function), they will always provide a better fit with respect to the common rupture duration model. An F test can than be used to evaluate the misfit improvement versus the increase of degrees of freedom. F values above 0.5 will be used here to prefer unilateral or bilateral models with respect to the point source solution. The modelling of asymmetric bilateral rupture requires more free parameters, being the superposition of two functions as in Eq. 5. Chances for the implementation of such a model are highly limited by several factors, including data quality, focal mechanism, epicentral azimuthal coverage and local structural heterogeneities. We suggest here the adoption of this model only for specific cases rather than its implementation within the automated processing.

The major advantages of the presented approach are that only point source synthetic seismograms are used, so that forward modelling and inversion are fast. A second advantage lies in the intrinsic simplicity of this approach, which provides simple plots of easy interpretation and suggest its implementation for automated routines. In the worse case, if no clear pattern is detected, the retrieved information can still be used to better focus a more detailed full waveform kinematic inversion (e.g., as in Cesca et al. 2010), by limiting the range of rupture times and/or spatial extension to be tested. A last important advantage resides in the coherency of the inversion approach: we use the same tools and the same data to derive first the focal mechanism (or moment tensor) and to detect directivity effects, instead of relying on an externally calculated focal mechanism solution, which may be biased by a specific selection of stations, earth model, and processing routines. An important limitation of the method applicability is represented by a specific range of earthquake magnitudes. For small earthquakes, with the rupture process occurring in less than 2 s, the variation of the apparent rupture duration could be only detected by fitting high frequency spectra (up to 0.5 Hz or above), which requires a detailed knowledge of the crustal structure, and possibly the adoption of 3D earth models. On the opposite side, large earthquakes may present more complex rupture processes, with different slip patches or asperities, breaking at different times. Large earthquakes also present significant discrepancies between hypocentral and centroid locations. Both effects are not considered in our model and can then lead to erroneous interpretations. As a rule of thumb, we believe that earthquakes with magnitudes in a range Mw 5.5–7.0 may be the best suited for a successful application.

3 Synthetic tests for linear and planar sources

Before applying the method to real data, and in order to assess the method performance, we carry out a set of inversions using synthetic datasets. We generate synthetic seismograms first for linear sources and consequently to planar ones. Considered source models present different significant focal mechanisms and directions of rupture propagation. Both synthetics for linear and planar sources are generated using the Kiwi tools (http://kinherd.org; Heimann 2010), assuming the PREM model (Dziewonski and Anderson 1981). The inversion is then carried out as described in the previous paragraph, assuming a spatial point source. Focal mechanisms, scalar moment and depth are retrieved at a first stage, by using the method described in Cesca et al. (2010), which has been here specifically modified in order to include the retrieval of the apparent rupture time at each station. In the synthetic tests, a dense grid of 154 stations is considered, in order to plot apparent duration contours. Stations location accomplish to the chosen conditions in terms of epicentral distances.

Three line source mechanisms (strike-slip (SS) strike $\varphi = 30$, dip $\delta = 90$, rake $\lambda = 0$; normal fault (NF) $\varphi = 30$, $\delta = 45$, $\lambda = 90$; thrust fault (TF) $\varphi = 30$, $\delta = 20$, $\lambda = -90$) and three rupturing models (pure unilateral, asymmetric bilateral, pure bilateral) are considered at first, thus providing a set of nine source models. Ruptures propagate horizontally for the strike-slip and normal fault, in direction NNE–SSW, and toward ESE along the low-angle dipping plane, for the thrust fault. The source model centroid is always located at a depth of 20 km, the source length is 30 km, rupture velocity is 3.5 km/s. Pure unilateral ruptures start at the southern (SS, NF) or western (TF) edge. The same main rupture direction is used for asymmetric bilateral ruptures, the two ruptured segments having lengths $L_1 = 22.5$ and $L_2 = 7.5$ km. Rise time is fixed to 2 s in all cases. The inversion is carried out using 40 s time windows, starting 10 s before the theoretical arrival of P phases. A frequency bandpass, between 0.01 and 0.5 Hz, is used to filter Green's functions and data. Inversion results are shown in Fig. 3. Coloured surface, representing the inverted apparent source duration, highlight the radiation patterns of apparent duration. The azimuthal distribution of apparent duration clearly shows directivity effect and its minor dependence on epicentral distance using our approach and proof that a good quality fit can be achieved using the simplified azimuthal dependent curves. In particular, the fit of the cosine curve described by Eq. 5 can be used to detect unilateral or asymmetric bilateral ruptures, while the curve from Eq. 6 to detect pure bilateral ruptures. Rupture directivity is correctly detected in all cases, with the exception of the bilateral rupture along the low-dipping angle plane of the thrust mechanism (Fig. 3, bottom right), where unilateral rupture is incorrectly estimated. The reason for this discrepancy can be described as follows. Since the extended source is not horizontal, the segment toward ESE and WNW are located below

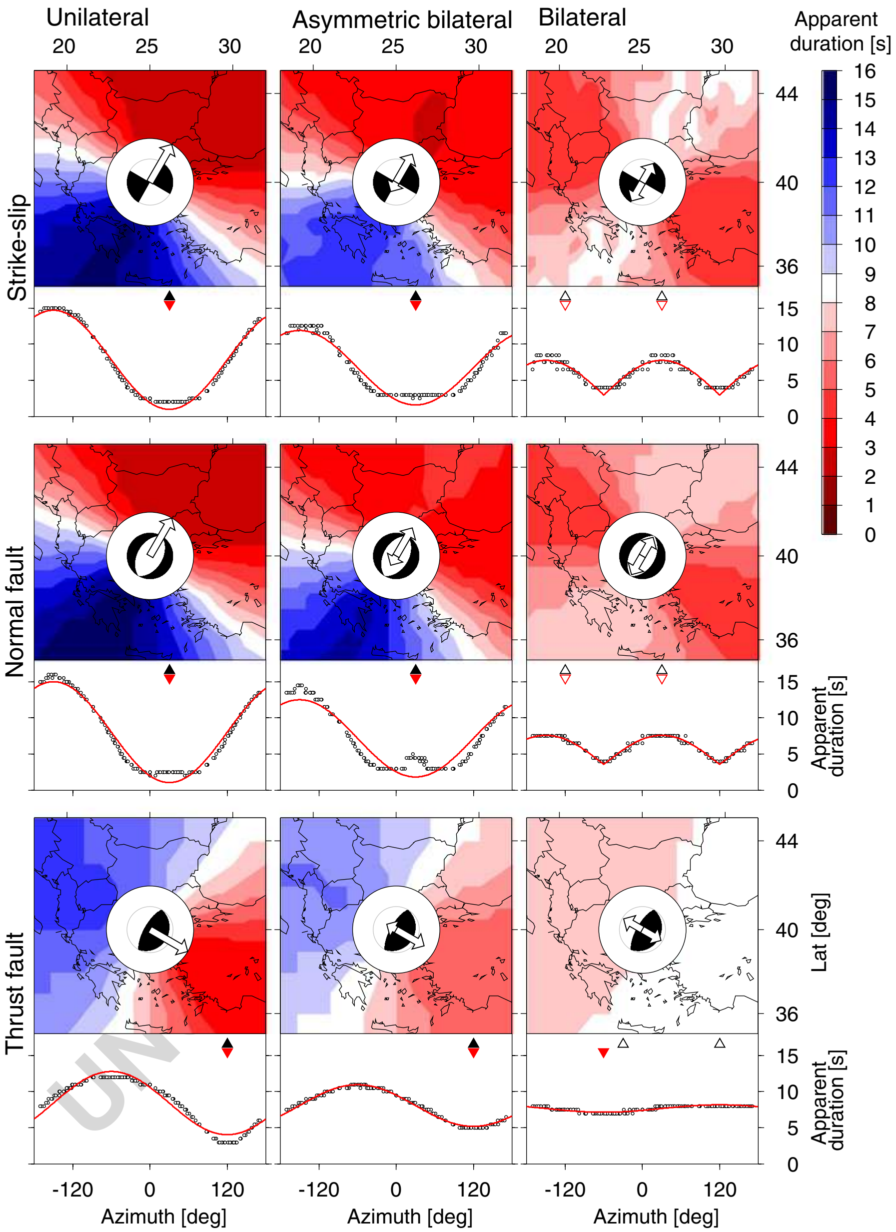

Fig. 3 Inversion results for linear sources. We consider three focal mechanisms (strike-slip, *top*; normal fault, *centre*; thrust fault, *bottom*) and three rupture processes (pure unilateral, *left*; asymmetric bilateral, *centre*; pure bilateral, *right*). For each case, we show colour plots representing the inverted apparent duration at a dense grid of station around the epicentre (*red to blue scale* represents increasingly longer apparent durations). The focal mechanisms are shown at the epicentral location, together with *white arrows* describing rupture directions (*arrow sizes* are proportional to rupture lengths). *Graphics below each colour plot* represent the apparent duration versus azimuth (*dots*) and the best fitting model (*red curves*). *Upper triangles* represent the correct solution (a *single black triangle* is plotted at the proper azimuth for unilateral and asymmetric bilateral ruptures; *two white triangles* indicate rupture directions for pure bilateral rupture cases). *Inverted triangles* represent inversion results (*single red triangle* for unilateral and asymmetric bilateral ruptures, *two white triangles* for pure bilateral ruptures)

and above the centroid depth, respectively. Since we use a layered model, the frequency content of synthetic seismogram varies from shallower to deeper sources, as well as take off angles. These effects, which cannot be reproduced by a point source located at the centroid depth, results larger than those related to the bilateral rupture, thus explaining the detection of an apparent directivity towards dip direction.

Given the successful application to line sources, we simulate now more realistic rupture processes, generating synthetic seismograms for the eikonal source model (Heimann 2010; Cesca et al. 2010). We use here circular faults, with rupture propagating with a variable velocity, scaling by a coefficient 0.9 with shear wave velocity in the crustal model. Given the adoption of the PREM model, the source depth and its extension, rupture velocity

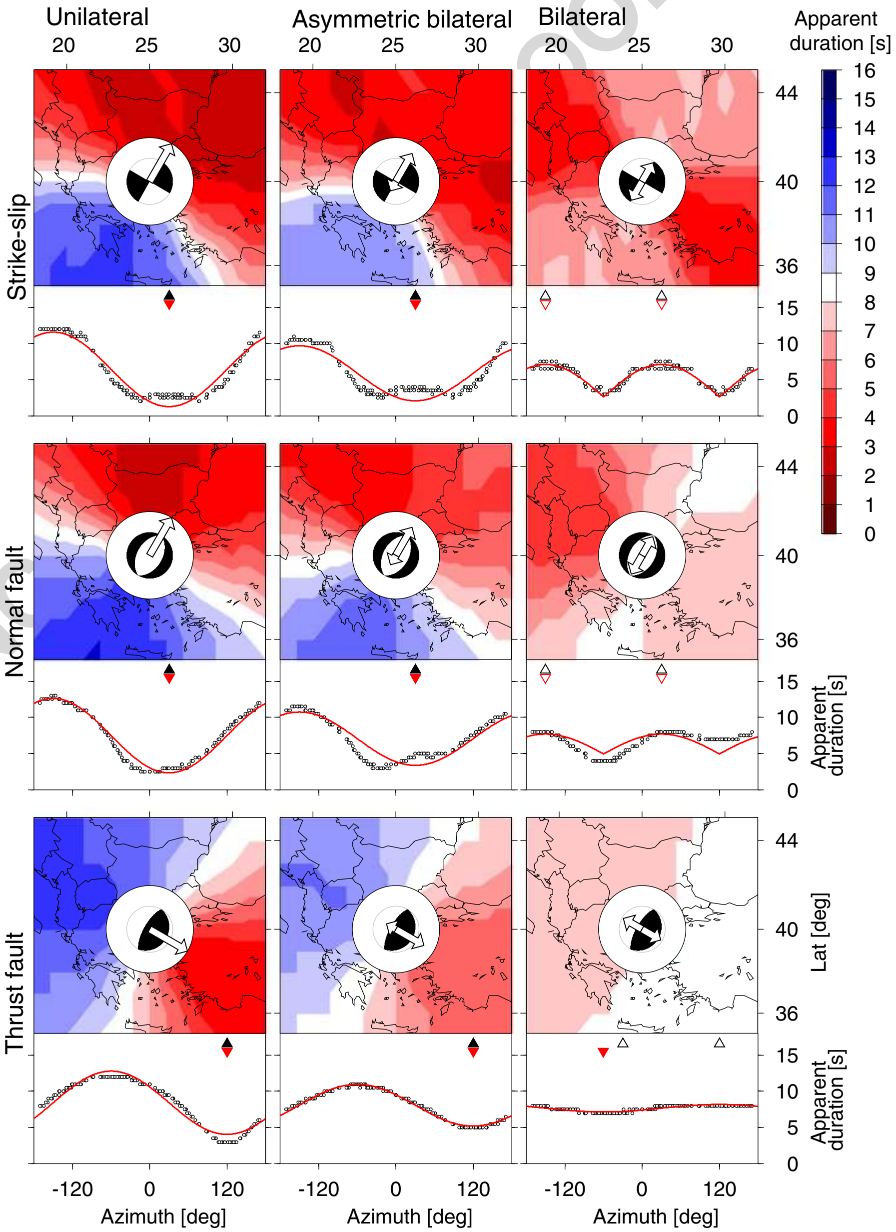

Fig. 4 Inversion results for circular eikonal sources. For each of the nine considered source models, we show colour plots representing the inverted apparent duration around the epicentre (*red to blue scale* represents increasingly longer apparent durations). Graphics below each coloured plot represent the apparent duration versus azimuth (*dots*) and the best fitting model (*red curves*). We use the same symbol convention as in Fig. 3

range between 2.9 and 4.0 km/s. Inversion is carried out using the same approach and parameters as for the previous test and results summarized in Fig. 4. The main characteristics of the azimuthal patterns of the apparent rupture duration are preserved. Directivity effects can be detected and modelled for all pure unilateral and asymmetric bilateral ruptures, although the fit quality results in some cases significantly poorer than for line source cases. The adoption of bi-dimensional ruptures, and specifically the inclusion of sources at different depths, slightly modifies the apparent duration pattern, as can be seen by the comparison of plots in Figs. 3 and 4 relative to normal fault mechanism. The modification of the apparent rupture radiation pattern has similar causes than those described for linear sources. Additionally, it is here also depending on the variable rupture velocity (which, according to the crustal model, is faster for deeper sources than for shallower ones). These effects result critical for the inversion of a bilateral rupture for the case of a thrust fault mechanism, which is erroneously interpreted as unilateral (with a rupture propagation in dip direction). On the other hand, the discrimination between pure and asymmetric bilateral rupture is not always possible; the observation of the characteristic lobe associated to the asymmetric bilateral rupture may indicate such a rupture process, but could not be sufficient, alone, to distinguish this case to a pure unilateral rupture.

A variation of the scalar moment will lead to a scaling of synthetic seismograms and modify their amplitude spectra. As a consequence, the inversion of apparent durations may lead to slightly different results. In order to investigate these effects, we have perturbed the scalar moments used for synthetic tests, and analyse inversion results. While the uni- or bilateral mode of the rupture and the main rupture direction are not influenced by a variation of the scalar moment and are always correctly retrieved, the rupture time and the following estimation of rupture lengths suffer slight changes. A perturbation of 10% of the correct scalar moment always led to uncertainties below 5% in terms of rupture time and rupture length. Synthetic tests suggest the implementation of the method here proposed towards a rapid detection of directivity effects. Additionally, these tests point out specific cases, where the inversion approach results more critical, and where a careful discussion of results is suggested. In general, horizontal ruptures and pure or partially unilateral ruptures are more easily detected, whereas pure bilateral sources and rupture propagating along dipping directions may be more problematic to resolve.

4 The Andravida 8.6.2008 earthquake

On June 8th, 2008, a magnitude Mw 6.4 earthquake struck NW Peloponnese, Greece. The earthquake, here further referred as the Andravida earthquake, produced two casualties, about 100 injuries and several damages (Chouliaras 2009). A wide number of studies covered the earthquake source and its effects. A pure strike-slip focal mechanisms was unanimously provided by several institutions and catalogues surveying regional and global seismicity, including National Observatory in Athens (NOA), Aristotle University of Thessaloniki (AUTH), INGV European-Mediterranean RCMT Catalogue (INGV-RCMT), Swiss Federal Institute of Technology, United States Geological Survey (USGS) and Global CMT Catalogue (CMT). According to these models, fault planes are almost vertical and oriented NNE–SSW and WNW–ESE. Source depth estimations showed some variability, ranging between 10 and 38 km, and magnitudes Mw ranged between 6.3 and 6.5. The epicentral locations of the earthquake aftershocks (Ganas et al. 2009; Gallovic et al. 2009; Kostantinou et al. 2009), which are distributed within a narrow strip extending NNE–SSW, provide a convincing image of the rupture orientation. The cloud of aftershocks elongates for about 30–35 km, providing a first rough estimation of rupture size. The aftershock distribution is denser towards the Northern edge. To the south, epicentral locations may indicate a minor bending of the rupture area to a slightly larger strike. All published source models are consistent with the identification of the NNE–SSW striking fault plane. Sokos et al. (2008), using hypocentral-centroid relative location method, identified the same plane; since centroids locations are generally located North of hypocentral locations, some indication for a dominant propagation towards North may arise from this study. Even more convincing, with respect to the detection of directivity, are the studies of Kostantinou et al. (2009), Gallovic et al. (2009) and Cesca et al. (2010). The first authors derived a finite source model, also consistent with their aftershock relocations, finding a rupture length of 22.4 km and an asymmetric bilateral rupture, with a major rupture along the NE branch. Gallovic et al. (2009) used a conjugate gradient method to detect the spatio-temporal evolution of the rupture process. Results indicate a predominantly unilateral rupture, propagating along a main slip patch, with a rupture length of about 20 km and a rupture velocity of about 3 km/s. Cesca et al. (2010), based on amplitude spectra inversion of full waveform and assuming an eikonal source model, detected an asymmetric rupture propagation, with a predominance of rupture propagation towards NNE; the rupture length was estimated 40 km, while the average rupture velocity was fixed to about 3.2 km/s. The consistency of these results (see Fig. 5 bottom), obtained with different methods and datasets, offer a serious reference to our study in terms of fault plane identification and rupture directivity.

In our inversion, we assume the epicentral location provided on the EMSC-CSEM webpage and the focal mechanism determined by Cesca et al. (2010), which is based on the fit of full waveform amplitude spectra. We observed that a new estimation of the scalar moment, based on the fit of P wave spectra only, would present minor variation with respect to the assumed value (5.97e18 instead of 6.07e18 Nm). Then, we invert

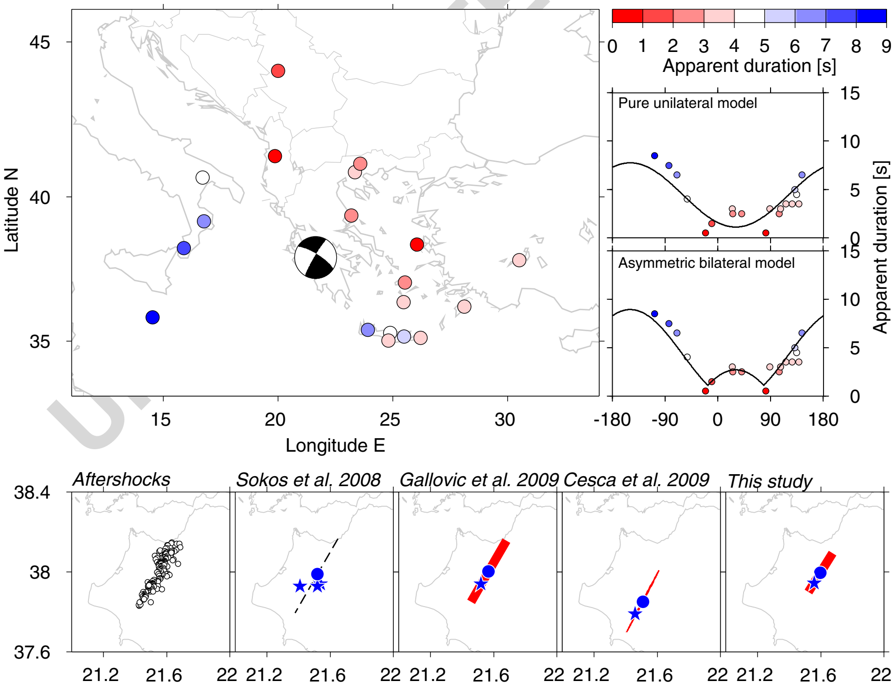

Fig. 5 Inversion results for the Mw 6.4 Andravida (NW Peloponnese) earthquake (*top*) and comparison with published source models (*bottom*). *Top*: coloured dots represent the inverted apparent duration at the stations used, according to the given colour scale; the azimuthal distribution of apparent durations may be fitted (*top right*) assuming a pure unilateral or, better, a partially unilateral rupture (*thick lines*). *Bottom*: the comparison of aftershocks distribution (after Gallovic et al. 2009) identifies the NNE–SSW rupture plane in agreement with centroid-hypocentral technique (Sokos et al. 2008), adjoint method (Gallovic et al. 2009), full waveform kinematic inversion (Cesca et al. 2010) and our results; the last four methods consistently detect a partially unilateral rupture towards NNE. *Stars* and *blue circles* represent here nucleation points and centroids respectively; the rupture area is plotted in *red*

for the apparent duration at each station separately and plot resulting values in function of station azimuth (Fig. 5), according to the discussed methodology. As a first approximation, we try to fit apparent durations by means of pure unilateral and pure bilateral rupture models, assuming both fault planes. Since fault planes are almost vertical, only horizontal directions of the rupture velocity along these planes are considered. The unilateral rupture model with rupture propagation towards NNE provide a very good fit to the apparent duration data, and is preferred to remaining models on the base of the F test. This result provides a clear indication for a rupture propagating towards NNE, and thus can be used to discriminate the true fault plane (NNE–SSW) from the auxiliary one (WNW–ESE). Based on the good fit, we try to refine our solution by investigating asymmetric bilateral ruptures. Results provide an even more convincing fit (Fig. 5, bottom right), when an asymmetric bilateral source model with rupture propagating mostly Northward is assumed, as the curve account for the two symmetric minima at about −21.5 and 82.5° and the internal characteristic lobe of asymmetric rupture (see Fig. 2, bottom). On the other side, this result is in very good agreement with published models discussed before. According to the previous discussion for a simplified bidimensional case, the maxima of the two cosine curves associated to the rupturing of two segments of the fault are equal to $t_\mathrm{P} + t_\mathrm{R} + t_r$, where these terms refer to the P wave propagation, rupture and rise time related to each segment. The maxima of the apparent duration curve are equal to 8.9 s (segment L_1 toward NNE) and 2.7 s (segment L_2 toward SSW). Assuming an average P wave velocity of 8 km/s (consistent with the used velocity model at the hypocentral depth), a rupture velocity of 3 km/s (consistent with Gallovic et al. 2009), and considering the rise time negligible with respect to rupture time, we obtain rupture lengths of about 19 and 6 km. The total length of about 25 km for the main patch is in general agreement with most of published results. We observe a discrepancy with the rupture size of about 40 km determined in Cesca et al. (2010). This last value might be overestimated, as the adopted full waveform kinematic inversion may in some cases be affected by a trade-off between different source parameters. The observed discrepancy may also indicate a different response of the two approaches to the rupture process and energy emission, with the full waveform inversion detecting the largest rupture length, and the directivity inversion identifying the main rupture patch. The upper limit value we found here is slightly larger than the length estimated by standard empirical relations (according to Wells and Coppersmith 1994, the average rupture length for a Mw 6.4 is about 14 km). We remark that the interpretation of inversion results to this extent should be carried out only in best conditions, where the fitting of the apparent duration curve is good enough to further interpret it.

5 The SW Peloponnese 14–20.2.2008 seismic sequence

A seismic sequence struck the region offshore SW Peloponnese, Greece, in the days following February 14th, 2008, with three major earthquakes occurring within a week. On February 14th, a first Mw 6.8 (magnitude estimated by EMSC-CSEM and Cesca et al. 2010) event struck the region at 10:09 UTC. Two hours later, at 12:08, UTC, a Mw 6.2 aftershock occurred. Finally, on February 20th (18:27 UTC), a Mw 6.2 event took place. Focal mechanisms (EMSC-CSEM webpage) indicate thrust faulting for the first two events, while the last one has a different, strike-slip mechanism, with fault planes striking ENE and NNW. Source depths, according to EMSC-CSEM catalogue, were 30, 20 and 25 km, respectively, for the three earthquakes. Whereas different institutions (e.g. NOA, AUTH, University of Patras UPSL, INGV-RCMT, USGS, CMT) provided point source solutions for these events, few trials has been carried out so far to interpret rupture kinematics (Roumelioti et al. 2009; Cesca et al. 2010). A strongly uneven station distribution and large epicentral gaps toward SW have possibly limited source modelling until now. Based on full waveform inversion, Cesca et al. (2010) identified the ENE–WSW plane for the strike-slip earthquake of February 20th, and a partial unilateral rupture towards the coast was found. For the first two earthquakes, the low angle planes dipping toward NW were preferred, but the inversion results were not completely satisfactorily. Roumelioti et al. (2009) adopted an empirical Green's functions approach, using the Mw 6.2 aftershock to model the finite fault of the largest earthquake; their results support the identification of the low angle dipping plane as well as directivity towards SSW. Finally, the identification of low dip angle rupture planes in this region for thrust earthquakes would agree with local tectonics, associating the earthquake occurrence to oceanic subduction (Underhill 1999).

Figure 6 summarizes our inversion results. Differently from the application to the Andravida earthquake, apparent durations for the earthquakes occurring on February 14th show a major spreading and are worse fitted by the simplified cosine function we associated to pure unilateral ruptures. A better fit, and minor spreading, is observed for the main event, with respect to its aftershock. However, for both two earthquakes, a general trend can be detected, indicating a minimum of the cosine curve for an azimuth of about 135°, which suggests a main direction of the rupture propagation towards SE. These results are unable by themselves to provide further informations about the true fault plane, as they may be modelled either assuming the low-angle and the steep dipping plane. A better fit is obtained for the February 20th earthquake: clear directivity effect

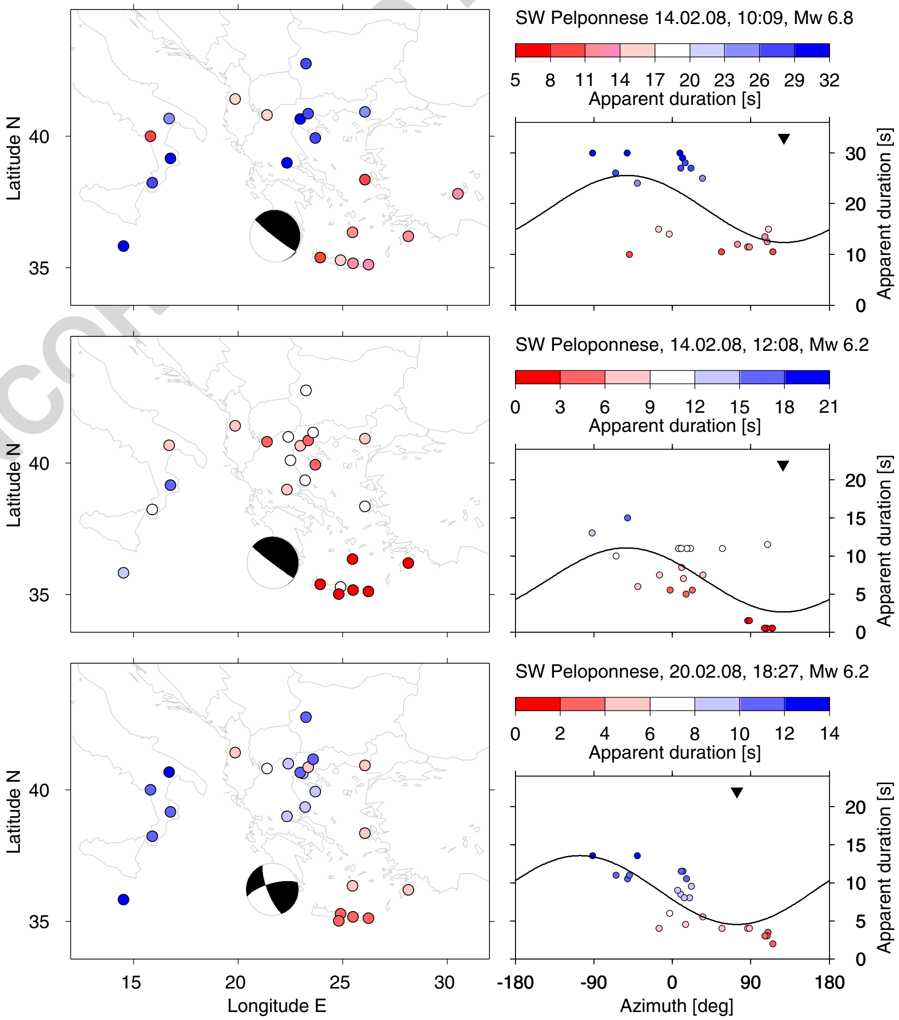

Fig. 6 Inversion results for the February 14th, 2008, Mw 6.8 (*top*), the February 14th, 2008, Mw 6.2 (*centre*) and the February 20th, 2005, Mw 6.2 (*bottom*) earthquakes, offshore SW Peloponnese. For each earthquake, *coloured dots* represent the inverted apparent duration at the stations used, according to the colour scale given for each case; the azimuthal distribution of apparent durations (*right*) may be fitted assuming unilateral ruptures (*thick black lines*). *Inverted triangles* indicate the retrieved rupture directions

is here retrieved, indicating a rupture mostly propagating towards ENE, thus along the WSW–ENE fault plane. The differentiation between pure or partial unilateral rupture may be here rewarded as beneath the limit of a safe data interpretation, but we observed how the general result is in well agreement with previous results by Cesca et al. (2010), where the source model was derived by the fit of high-frequency (up to 0.1 Hz) amplitude spectra from the whole waveforms.

Finally, we investigate effects of the assumption of imprecise point source parameters on the estimation of rupture directivity. The effects of anomalous source depth estimation are studied for the February 20th aftershock, as different Institutions have provided a range of different values ranging from 8 to 25 km. We repeated the inversion using a different point source solution (strike 249°, dip 88°, rake −12°, depth 12 km), as provided by the INGV European-Mediterranean RCMT Catalog; this focal mechanism is similar to our solution and major differences concern centroid depth, which is now shallower. Directivity inversion remains very stable, showing a consistent identification of unilateral rupture direction toward SE, and indicates that a source depth variation of about 10km does not result in any significant variation in the radiation pattern of apparent duration. In a similar way, we tested slightly different focal mechanisms for both earthquakes of February 14th: even if our focal mechanisms are in relatively good agreement with other published solutions, some difference can be observed. For example, the INGV-RCMT catalogue indicates strike angles of 333° and 298°, for these earthquakes, which differ from our solution (347° and 341° respectively). Even in this case, after adopting the source parameters provided by INGV-RCMT, the inversion results are stable, with the detection of main rupture directions pointing towards SE–ESE.

6 Conclusions

We propose here a new method for a quick detection of directivity effects for shallow earthquakes at regional distances. Among the most important features of the method, we highlight here the following ones:

- Rapid inversion

The assumption of spatial point source allows an extremely rapid generation of synthetic seismograms and point source parameters inversion, thus offering a tool to early detect directivity; to quantify such improvement, on a standard single processor PC the inversion of directivity is here carried out within a minute, about 20 times faster than the full kinematic inversion for the same event, using the approach described in Cesca et al. (2010).

- Coherent inversion

The use of the Kiwi tools for data processing and inversions improves significantly the consistency of our methodology: for example, the same dataset and the same inversion tools can be used to first derive the focal mechanism, then the scalar moment and finally the apparent duration; we believe this consistency between data used for different inversions significantly improve the coherency of the inversion approach.

- Accounting for wave propagation

The method is based on amplitude spectra inversion, using theoretical Green's functions for the chosen earth model. In this way, we account for wave propagation effect, an improvement with respect to standard methods based on pulse length estimations.

- No requirements of specific aftershocks

Avoiding the use of empirical Green's function, the method is not limited by the existence of a proper aftershock, nor need to wait for its occurrence.

- Automation

The adoption of the Kiwi tools and the simplicity of the inversion approach made possible the implementation of the method as automated routine.

In this manuscript we have demonstrated the method performance, both with a range of synthetic tests and with observed data for different shallow earthquakes recently occurred. These applications offer indications about the quality and extent of inversion results. The retrieval of pure unilateral and pure bilateral ruptures is in general better resolved than asymmetric ruptures, although the application to the June 8th, 2008, Andravida earthquake showed that this case can also be detected, in favourable conditions. In general, directivity effects are better resolved for strike slip earthquakes, with respect to normal or thrust faulting. Directivity detection offers often a chance to identify the rupture plane, discriminating it from the auxiliary one. The determination of rupture time, rise time and rupture velocity on the base of the proposed method is beyond its purposes and should require a careful supervision. We have here focused to earthquake with magnitudes of Mw 6 to 7 and shallow hypocentres. The extension of this inversion approach for the study of other range of magnitudes or deeper sources may be investigated in future.

Acknowledgements We thank Prof. J. Zahradnik and two anonymous reviewers for useful comments and suggestions. The facilities of GEOFON and IRIS Data Management System, and specifically the IRIS Data Management Center, were used for access part of the waveform and metadata required in this study. We acknowledge all institutions providing seismic data used in this research: GEOFON, MEDNET Project, Greek National Seismic Network and Aristotle University Thessaloniki Network. Maps and focal mechanisms have been plotted with GMT (Wessel and Smith 1998). This work has been funded by the German DFG project KINHERD (DA478/14–1/2) and the German BMBF/DFG "Geotechnologien" project RAPID (BMBF07/343).

References

Beck SL, Silver P, Wallace TC, James D (1995) Directivity analysis of the deep Bolivian earthquake of June 9, 1994. Geophys Res Lett 22:2257–2260

Ben-Menahem A (1961) Radiation of seismic surface waves from finite moving sources. Bull Seismol Soc Am 51:401–453

Ben-Menahem A, Singh SJ (1981) Seismic waves and sources. Springer, New York

Bernard P, Madariaga R (1984) A new asymptotic method for the modelling of near-field accelerograms. Bull Seismol Soc Am 74:539–557

Beroza GC, Spudich P (1988) Linearized inversion for fault rupture behaviour: application to the 1984 Morgan Hill, California, earthquake. J Geophys Res 93:6275–6296

Boore D, Joyner W (1978) The influence of rupture incoherence on seismic directivity. Bull Seismol Soc Am 68:283–300

Brüstle W, Müller G (1987) Stopping phases in seismograms and the spatiotemporal extent of earthquakes. Bull Seismol Soc Am 1:47–68

Caldeira B, Bezzeghoud M, Borges JF (2009) DIRDOP: a directivity approach to determining the seismic rupture velocity vector. J Seismol 14:565–600. doi:10.1007/s10950-009-9183-x

Cassidy JF (1995) Rupture directivity and slip distribution for the Ms 6.8 earthquake of 6 April 1992, Offshore British Columbia: an application of the empirical Green's function method using surface waves. Bull Seismol Soc Am 85:736–746

Cesca S, Heimann S, Stammler K, Dahm T (2010) Automated procedure for point and kinematic source inversion at regional distances. J Geophys Res 115:B06304. doi:10.1029/2009JB006450

Chouliaras G (2009) Seismicity anomalies prior to 8 June 2008, Mw 6.4 earthquake in Western Greece. Nat Hazards Earth Syst Sci 9:327–335

Dahm T, Krüger F (1999) Higher-degree moment tensor inversion using far-field broad-band recordings: theory and evaluation of the method with application to the 1994 Bolivia deep earthquake. Geophys J Int 137:35–50

Dahm T, Kruger F, Stammler K, Klinge K, Kind R, Wylegalla K, Grasso JR (2007) The 2004 Mw 4.4 Rotenburg, Northern Germany, Earthquake and its possible relationship with Gas Recovery. Bull Seismol Soc Am 97:691–704

Dreger D, Kaverina A (2000) Seismic remote sensing for the earthquake source process and near-source strong shaking: a case study of the October 16, 1999 Hector mine earthquake. Geophys Res Lett 27:1941–1944

Dziewonski AM, Anderson DL (1981) Preliminary reference earth model. Phys Earth Planet Int 25:297–356

Eshghi S, Zare M (2003) Reconnaisance report on 26 December 2003 Bam earthquake. International Institute of Earthquake Engineering (IIEES)

Gallovic F, Zahradnik J, Krizova D, Plicka V, Sokos E, Serpetsidaki A, Tselentis GA (2009) From earthquake centroid to spatial-temporal rupture evolution: Mw 6.3 Movri Mountain earthquake, June 8, 2008, Greece. Geophys Res Lett 36:L21310. doi:10.1029/2009GL040283

Ganas A, Serpelloni E, Drakatos G, Kolligri M, Adamis I, Tsimi C, Batsi E (2009) The Mw 6.4 SW-Achaia (western Greece) earthquake of 8 June 2008: seismological, field, GPS, observations and stress modeling. J Earthq Eng 8:1101–1124

Hartzell SH (1978) Earthquake aftershocks as Green's functions. Geophys Res Lett 5:1–4

Hartzell S, Heaton DV (1983) Inversion of strong ground motion and teleseismic waveform data for the fault rupture history of the 1979 Imperial Valley, California, earthquake. Bull Seismol Soc Am 83:1553–1583

Hartzell S, Helmberger DV (1982) Strong-motion modelling of the Imperial Valley earthquake of 1979. Bull Seismol Soc Am 72:571–596

Haskell NA (1964) Total energy and energy spectral density of elastic wave radiation from propagating faults. Bull Seismol Soc Am 54:1811–1841

Heimann S (2010) A robust method to estimate kinematic earthquake source parameters. PhD Thesis, University of Hamburg, Germany, pp 145

Imanishi K, Takeo M (1998) Estimates of fault dimensions for small earthquakes using stopping phases. Geophys Res Lett 25:2897–2900

Imanishi K, Takeo M (2002) An inversion method to analyze rupture process of small earthquakes using stopping phases. J Geophys Res 107:ESE2.1–ESE2.16. doi:10.1029/2001JB000201

Kostantinou KI, Melis NS, Lee SJ, Evangelidis CP, Boukouras K (2009) Rupture process and aftershock relocation of the 8 June 2008 Mw 6.4 earthquake in Northwest Peloponnese, Western Greece. Bull Seismol Soc Am 99:3374–3389

Li Y, Toksöz MN (1993) Study of the source process of the 1992 Columbia Ms = 7.3 earthquake with the empirical Green's function method. Geophys Res Lett 20:1087–1090

Madariaga R (1977) High-frequency radiation from crack (stress drop) models of earthquake faulting. Geophys J R Astron Soc 51:625–651

Madariaga R (1983) High-frequency radiation from dynamic earthquake fault models. Ann Geophys 1:17–23

McGuire JJ, Zhao L, Jordan TH (2001) Teleseismic inversion for the second-degree moments of earthquake space-time distributions. Geophys J Int 145:661–678

McGuire JJ, Zhao L, Jordan TH (2002) Predominance of unilateral rupture for a global catalog of large earthquakes. Bull Seismol Soc Am 92:3309–3317

Müller CS (1985) Source pulse enhancement by deconvolution of empirical Green's functions. Geophys Res Lett 12:33–36

Nadim F, Moghtaderi-Zadeh M, Lindholm C, Andresen A, Remseth S, Bolourchi MJ, Mokhtari M, Tvedt T (2004) The Bam earthquake of 26 December 2003. Bull Earthquake Eng 2:119–153

Nielsen S, Madariaga R (2003) On the self-healing fracture mode. Bull Seismol Soc Am 93:2375–2388

Olson AJ, Apsel RJ (1982) Finite faults and inverse theory with applications to the 1979 Imperial Valley earthquake. Bull Seismol Soc Am 72:1969–2001

Pro C, Buforn E, Udías A (2007) Rupture length and velocity for earthquakes in the Mid-Atlantic Ridge from directivity effects in body and surface waves. Tectonophysics 433:65–79

Roumelioti Z, Benetatos C, Kiratzi A (2009) the 14 February 2008 earthquake (M6.7) sequence offshore south Peloponnese (Greece): source models of the three strongest events. Tectonophysics 471:272–284

Selby N, Eshun E, Patton H, Douglas A (2005) Unusual long-period Rayleigh wave from a vertical dip-slip source: the 7 May 2001, North Sea earthquake. J Geophys Res 110:B10304. doi:10.1029/2005JB003721

Sokos E, Serpetsidaki A, Tselentis GA, Zahradnik J (2008) Quick assessment of the fault plane, for the recent strike-slip event in the North-Western Peloponnese, Greece, (8 June 2008, Mw 6.3). EMSC-CSEM Report

Spudich P, Frazer LN (1984) Use of ray theory to calculate high-frequency radiation from earthquake sources having spatially variable rupture velocity and stress drop. Bull Seismol Soc Am 74:2061–2082

Underhill JR (1999) Late Cenozoic deformation of the Hellenide forelands, Western Greece. Geol Soc Am Bull 101:613–634

Vallée M (2007) Rupture properties of the giant sumatra earthquake imaged by empirical Green's function analysis. Bull Seismol Soc Am 97:103–114

Vallée M, Bouchon M (2004) Imaging coseismic rupture in the far field by slip patches. Geophys J Int 156:615–630

Velasco AA, Ammon CJ, Lay T (1994) Empirical green function deconvolution of broadband surface waves: Rupture directivity of the 1992 Landers, California (Mw = 7.3), earthquake. Bull Seismol Soc Am 84:735–750

Velasco AA, Ammon CJ, Farrell J, Pankow K (2004) Rupture directivity of the 3 November 2002 denali fault earthquake determined from surface waves. Bull Seismol Soc Am 94:293–299

Warren LM, Shearer PM (2006) Systematic determination of earthquake rupture directivity and fault planes from analysis of long-period P-wave spectra. Geophys J Int 164:46–62

Wells DL, Coppersmith KJ (1994) New empirical relations among magnitude, rupture length, rupture width, rupture area and surface displacements. Bull Seismol Soc Am 84:974–1002

Wessel P, Smith WHF (1998) New improved version of the generic mapping tools released. Eos Trans AGU 79:579

Zahradnik J, Gallovic F, Sokos E, Serpetsidaki A, Tselentis GA (2008) Quick fault-plane identification by geometrical method: application to Mw 6.2 Leonidio earthquake, January 6, 2008, Greece. Seismol Res Lett 79:653–662

AUTHOR QUERY

NO QUERY